

# Online Training and Inference System on Edge FPGA Using Delayed Feedback Reservoir

SOSEI IKEDA, Kyoto University, Japan

HIROMITSU AWANO, Kyoto University, Japan

TAKASHI SATO, Kyoto University, Japan

A delayed feedback reservoir (DFR) is a hardware-friendly reservoir computing system. Implementing DFRs in embedded hardware requires efficient online training. However, two main challenges prevent this: hyperparameter selection, which is typically done by offline grid search, and training of the output linear layer, which is memory-intensive. This paper introduces a fast and accurate parameter optimization method for the reservoir layer utilizing backpropagation and gradient descent by adopting a modular DFR model. A truncated backpropagation strategy is proposed to reduce memory consumption associated with the expansion of the recursive structure while maintaining accuracy. The computation time is significantly reduced compared to grid search. Additionally, an in-place Ridge regression for the output layer via 1-D Cholesky decomposition is presented, reducing memory usage to be 1/4. These methods enable the realization of an online edge training and inference system of DFR on an FPGA, reducing computation time by about 1/13 and power consumption by about 1/27 compared to software implementation on the same board.

CCS Concepts: • **Computer systems organization** → **Neural networks**.

Additional Key Words and Phrases: reservoir computing, delayed feedback reservoir (DFR), edge computing

## ACM Reference Format:

Sosei Ikeda, Hiromitsu Awano, and Takashi Sato. 0000. Online Training and Inference System on Edge FPGA Using Delayed Feedback Reservoir. *ACM Trans. Embedd. Comput. Syst.* 00, 0, Article 000 ( 0000), 25 pages. <https://doi.org/XXXXXXX.XXXXXXX>

## 1 INTRODUCTION

Reservoir computing (RC) is a machine learning method that utilizes a reservoir to nonlinearly transform inputs into a high-dimensional space [21]. Typically, the reservoir weights remain fixed, with only the weights of the output layer being subjected to training [14]. A delayed feedback reservoir (DFR) [3] is a specific RC variant, which incorporates a reservoir composed of a nonlinear element and a feedback loop. The nonlinear element commonly adopts a Mackey–Glass equation [15]. Various implementations of RC have been demonstrated, leveraging electronic circuits [3], optical elements [13], etc. Among RC architectures, the structural simplicity of DFR makes it an attractive candidate for embedded hardware implementation due to its low power consumption [21]. In addition, unlike most RC implementations, the reservoir weights in DFR can be adjusted through several parameters, resulting in superior accuracy compared to other RC architectures [10].

In the context of embedded applications, the concept of an online training and inference system on edge devices is of paramount importance. The edge system offers several benefits, including

---

Authors' addresses: Sosei Ikeda, Kyoto University, Kyoto, Japan, [sikeda@easter.kuee.kyoto-u.ac.jp](mailto:sikeda@easter.kuee.kyoto-u.ac.jp); Hiromitsu Awano, Kyoto University, Kyoto, Japan, [awano@i.kyoto-u.ac.jp](mailto:awano@i.kyoto-u.ac.jp); Takashi Sato, Kyoto University, Kyoto, Japan, [takashi@i.kyoto-u.ac.jp](mailto:takashi@i.kyoto-u.ac.jp).

Permission to make digital or hard copies of all or part of this work for personal or classroom use is granted without fee provided that copies are not made or distributed for profit or commercial advantage and that copies bear this notice and the full citation on the first page. Copyrights for components of this work owned by others than ACM must be honored. Abstracting with credit is permitted. To copy otherwise, or republish, to post on servers or to redistribute to lists, requires prior specific permission and/or a fee. Request permissions from [permissions@acm.org](mailto:permissions@acm.org).

© 0000 Association for Computing Machinery.

1539-9087/0000/0-ART000 \$15.00

<https://doi.org/XXXXXXX.XXXXXXX>

real-time capabilities, adaptability, and security [8]. By executing computation close to the data source, the system curtails data transmission and achieves swift response times. The system can be fine-tuned to suit the edge environment without necessitating prior offline training. Additionally, data processing can transpire without external data transmission, thereby minimizing exposure to potential threats. A common use case for such a system is predictive maintenance of factory equipment. Traditional preventive maintenance, conducted at regular intervals, often results in excessive or unnecessary upkeep. Ideally, potential equipment failures should be predicted by analyzing equipment data in real-time. The online edge system meets this need by providing real-time processing capabilities and specialized equipment fault estimation while concurrently ensuring the security of sensitive equipment.

To implement such a system using DFR, efficient optimization methods for reservoir weights and memory efficient linear regression methods are imperative. First of all, the time-intensive reservoir weight optimization impedes its online execution. The performance of RC heavily depends on reservoir weights or parameters [21]. Typically, parameter optimization in DFR relies on grid search [3], which confronts notable scalability challenges as the dimension of the parameter space increases. In DFR, both the regularization parameter of the linear regression at the output layer and the reservoir parameters necessitate simultaneous optimization. The objective function within the parameter space can exhibit substantial nonlinearity, mandating finely segmented grids and resulting in significant computational overhead. Additionally, the memory-intensive linear regression at the output layer obstructs its edge implementation. The number of features provided by the reservoir layer depends on the length of the input series. Consequently, the features must be converted into a reservoir representation with a fixed length [10]. The reservoir representation is a high-dimensional vector, approximately 1,000 in dimension, as it must encapsulate features from preceding time periods. Given that the reservoir representation acts as the input for the output layer, deriving its parameters entails computationally expensive operations, including the inversion of a matrix of corresponding size, such as 1,000 by 1,000. Storing this high-dimensional matrix and its inverse necessitates a considerable amount of memory.

This paper presents the application of backpropagation and gradient descent to the online optimization of the reservoir layer of DFR. Although backpropagation and gradient descent [2] are widely used and proven effective training methods for neural networks, to the best of the authors' knowledge, no prior study has applied them to DFR. There exist two challenges: the use of nonlinear element that are often based on physical phenomena that have no derivatives, and the recursive structure that requires unfolding and requires infinitely long backpropagation traces [16]. To address these challenges, the authors propose to leverage the concept of modular DFR [11]. The modular DFR model reduces the number of parameters in the reservoir layer and divides the nonlinear element into multiple blocks, making backpropagation easier to apply. In addition to using this model, the recursively defined reservoir state of the DFR, which serves as a feature for the output layer, is approximated. The authors demonstrate that this approach enables fast online training for DFRs.

The authors propose a hardware-friendly Cholesky decomposition for optimizing the output layer of edge DFR by proving that the matrix associated with Ridge regression, the most widely used and high-performance learning method, is symmetric and positive definite. We also present an in-place inversion procedure that uses a single 1-D array to save memory usage. This is achieved by carefully designing the update order of the matrix in the Cholesky decomposition and matrix inversion, allowing the original matrix and computed results to share the same array. In addition, introducing small buffer reduces memory access collisions during the sum-of-products operation and facilitates parallel processing, thereby increasing the operating frequency.

The major contributions of this work are summarized as follows:

Table 1. Symbol table

Symbol	Definition
$u(k)$	digital time series input
$i(t)$	analog signal with D-A conversion of $u(k)$
$m(t)$	masking signal
$j(t)$	masked signal of $i(t)$
$x(t)$	output of the nonlinear element
$\gamma$	input scaling
$\eta$	parameter of the nonlinear element
$f$	nonlinear function
$\theta$	time interval of virtual nodes
$\tau$	total delay of a feedback loop
$N_x$	number of virtual nodes; reservoir size
$T$	length of a time series
$\mathbf{r}$	reservoir representation
$N_r$	number of features in a reservoir representation
$\mathbf{y}$	output
$N_y$	number of classes
$W_{\text{out}}$	weight of output layer
$\mathbf{b}$	bias of output layer
$p$	parameter of modular DFR
$q$	parameter of modular DFR
$\mathbf{e}$	one-hot encoding of $\mathbf{y}$
$\beta$	regularization parameter
$s$	$N_x^2 + N_x + 1$
$L$	loss function

- (1) Online edge training and inference system of DFR with a novel and efficient parameter optimization for reservoir and output layers. The implementation on an FPGA demonstrated significant performance gain by approximately 1/13 and power consumption by about 1/27 compared to the software implementation.
- (2) Development of a fast and accurate parameter optimization method utilizing backpropagation and gradient descent by adopting a modular DFR model. The proposed method achieves accuracy comparable to traditional grid search while reducing computation time by 700x.
- (3) Proposal of an in-place Ridge regression for the output layer via 1-D Cholesky decomposition. The hardware implementation of this method reduces memory usage to 1/4 while maintaining the same accuracy as the traditional Gaussian elimination method.

The remainder of this paper is organized as follows. First, Section 2 reviews the general concept of DFR and the modular DFR model. Section 3 proposes the online end-to-end edge DFR system. As the key components of this system, a fast parameter optimization method and a memory-saving Ridge regression method are proposed. Section 4 presents the evaluation of the proposed calculation method and the online edge implementation of DFR. Finally, Section 5 concludes the paper.

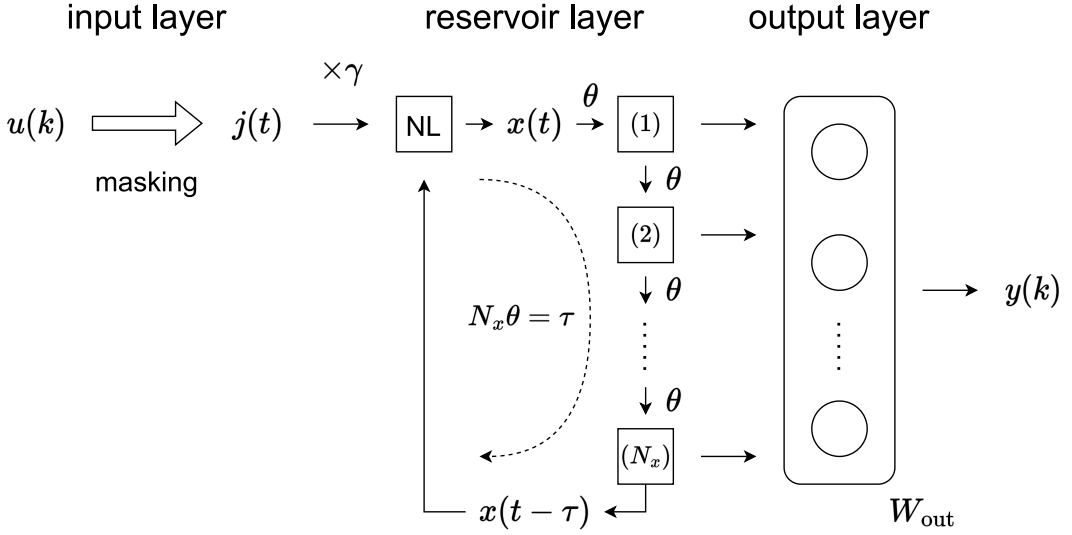


Fig. 1. Conceptual diagram of DFR. The reservoir consists of a NL and a feedback loop with a total delay  $\tau$ . The feedback loop comprises  $N_x$  virtual nodes with a time interval  $\theta$ .

## 2 DFR

First, the concept and basic operation of DFR are explained. Next, the dot-product reservoir representation (DPRR) [10], which enhances the accuracy of classification problems. Subsequently, we present the modular DFR model, which allows for more flexible design of nonlinear elements and incorporates backpropagation and gradient descent, offering an efficient alternative to time-consuming grid search. Finally, commonly used, memory-intensive output layer training methods are described. The symbols used throughout the discussion are listed in Table 1.

### 2.1 Concept of analog DFR

Reservoir computing is a machine learning scheme consisting of three layers: the input layer, the reservoir layer, and the output layer [14]. The input layer converts the input signal into a format suitable for entering the reservoir layer. The reservoir layer then transforms the signal into a high-dimensional nonlinear vector. Finally, the output layer performs pattern recognition using a simple learning algorithm. While the weights of the input and reservoir layers are fixed, the weights of the output layer are determined through training.

The DFR is a specific implementation of RC that incorporates a nonlinear element and a delayed feedback loop. Its structure captures past inputs, making it particularly suitable for processing time series data [21]. Due to its simplicity, DFR is considered more suitable for hardware implementation than other RC schemes [21]. Typically, hardware realizations of DFRs employ analog circuits in the reservoir layer [3, 20].

To demonstrate the operation and challenges of DFR, we begin with the most standard analog implementation. Fig. 1 illustrates a conceptual schematic of the DFR. The digital time-series input,  $u(k)$ , sampled at a period  $\tau$ , is first converted into an analog signal,  $i(t)$ . This signal then undergoes masking, where it is multiplied by the mask signal with a faster sample rate  $\theta$ . Fig. 2 depicts the most frequently used mask signals generated by a pseudo-random bit sequence. However, other masks may also be employed [3, 4]. The resulting signal  $j(t)$  is then scaled by  $\gamma$ , combined with the reservoir feedback, and passed through a nonlinear element (NL) to produce the output,  $x(t)$ .

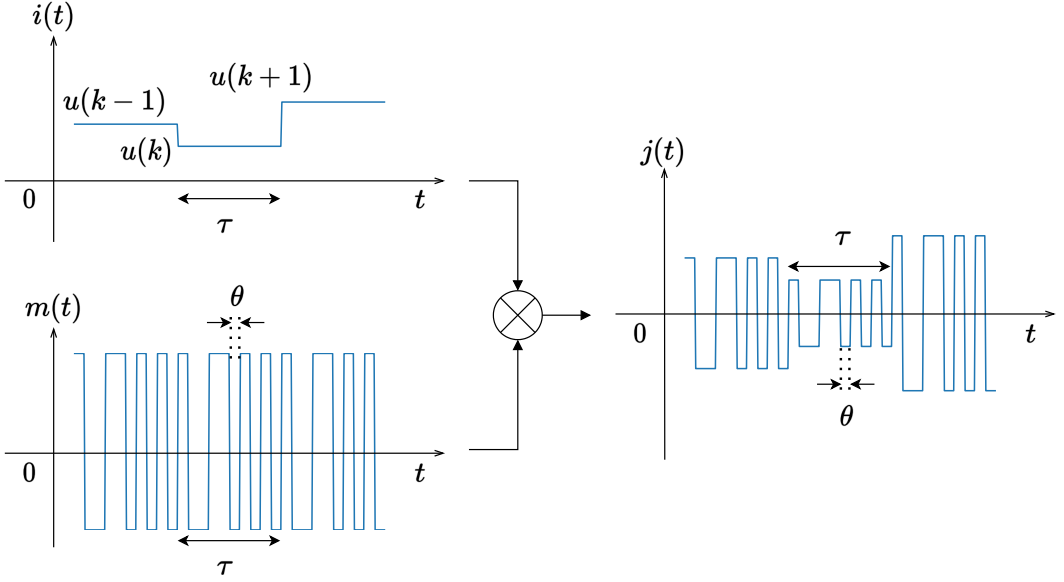


Fig. 2. Masking process.  $i$  is obtained by digital-to-analog conversion of input signal  $u$ . Signal  $i$  is constant at all  $\tau$ . Mask signal  $m$  takes different values at all time intervals  $\theta$ , and its period is  $\tau$ . Input signal to reservoir is expressed as  $j(t) = i(t) \cdot m(t)$ .

The NL is mathematically represented by the following delay differential equation:

$$\frac{d}{dt}x(t) = F(x(t - \tau), \gamma j(t)). \quad (1)$$

The Mackey–Glass model [15] is a commonly used NL in various studies [1, 3, 20]. Its operation is expressed by the following equations:

$$\frac{d}{dt}x(t) = -x(t) + \eta f(x(t - \tau), \gamma j(t)), \quad (2)$$

$$f(x(t - \tau), \gamma j(t)) = \frac{[x(t - \tau) + \gamma j(t)]}{1 + [x(t - \tau) + \gamma j(t)]^p}. \quad (3)$$

Here,  $p$  is an adjustable parameter.

A feedback loop with a total delay of  $\tau$  comprises virtual nodes spaced at regular time intervals of  $\theta$ . The signal values at these virtual nodes serve as the features and are collected as a vector of  $N_x$  elements, referred to as the reservoir state, where  $N_x \theta = \tau$ . The number of virtual nodes  $N_x$  is also referred to as the reservoir size.

The reservoir state is defined as follows:

$$\mathbf{x}(k) \equiv [x(k\tau - \theta), x(k\tau - 2\theta), \dots, x(k\tau - \tau)]. \quad (4)$$

The output, representing the inference result, is obtained by applying a linear transformation of the output layer to the reservoir state. The detailed methods for this process are described in Sections 2.3 and 2.5.

## 2.2 Concept of digital DFR

Fully digital versions of DFRs have been proposed to ease implementation [1, 3]. In these digital DFRs, the signal,  $j(k)$  after the masking process is expressed as  $j(k) = \mathbf{m}u(k)$  where  $\mathbf{m}$  is a mask vector of length  $N_x$  and its elements are determined randomly and digitally [3].

After masking, the nonlinear element and feedback loop of the DFR determine the reservoir state,  $\mathbf{x}(k)$ . Assuming that  $f$  in Eq. (2) is constant for a short time  $\theta$ , which is the time interval between the virtual nodes, the differential equation in Eq. (2) is solved for  $x(t)$  as follows:

$$x(t) = x_0 e^{-t} + \eta(1 - e^{-t})f(x(t - \tau) + \gamma j(t)), \quad (5)$$

where  $x_0$  is the initial value of  $x(t)$  at each  $\theta$  [3]. The value of the next virtual node can be expressed as  $x(\theta)$ . Assuming that the components of  $\mathbf{x}(k)$  and  $j(k)$  are

$$\mathbf{x}(k) \equiv [x(k)_1, x(k)_2, \dots, x(k)_{N_x}], \quad (6)$$

$$\mathbf{j}(k) \equiv [j(k)_1, j(k)_2, \dots, j(k)_{N_x}], \quad (7)$$

$\mathbf{x}(k)$  is obtained recurrently as follows:

$$\begin{aligned} x(k)_1 &= x(k-1)_{N_x} e^{-\theta} \\ &\quad + (1 - e^{-\theta})f(x(k-1)_1, j(k)_1), \end{aligned} \quad (8)$$

$$\begin{aligned} x(k)_n &= x(k)_{n-1} e^{-\theta} \\ &\quad + (1 - e^{-\theta})f(x(k-1)_n, j(k)_n). \quad (n \geq 2) \end{aligned} \quad (9)$$

The reservoir state is initialized to zero. The construction and operation of the output layer remain identical to those in the analog implementation.

In both implementations, grid search is the only effective method for parameter optimization due to the recursive nature of the network construction and the differentially defined NL.

## 2.3 DPRR

In classification tasks involving time-series inputs, a single output is generated at the end. To ensure consistency, the features obtained by the reservoir should be converted to an intermediate representation with a fixed length, known as the *reservoir representation* [10]. This conversion enables the features to be processed by an output layer of a fixed size [9].

Numerous reservoir representations have been proposed [3, 6, 7, 9, 17]. Currently, DPRR is considered to be the best in terms of both accuracy and circuit size [10]. Let the elements of  $\mathbf{x}(k)$  (i.e., the features) be  $[x(k)_1, x(k)_2, \dots, x(k)_{N_x}]$ . The vector of a node in the reservoir:

$$\mathbf{x}_n \equiv [x(1)_n, x(2)_n, \dots, x(T)_n], \quad (10)$$

can be considered to be the time evolution of the node state. Here,  $T$  denotes the length of a time series. Taking the dot product of these vectors for two nodes yields:

$$\mathbf{x}_i \cdot \mathbf{x}_j^- = \sum_{k=1}^T x(k)_i x(k-1)_j \quad (i, j = 1, 2, \dots, N_x). \quad (11)$$

In addition, the reservoir state itself is included as a feature:

$$\mathbf{x}_i \cdot \mathbf{1} = \sum_{k=1}^T x(k)_i \quad (i = 1, 2, \dots, N_x). \quad (12)$$

The DPRR is defined as a vector  $\mathbf{r}$  by concatenating Eqs. (11) and (12), which consists of  $N_x \cdot (N_x + 1)$  values, i.e.,  $\mathbf{r} \equiv \text{vec} \left( \sum_{i=1}^T \mathbf{x}(k) \mathbf{x}'(k-1) \right) \equiv [r_1, r_2, \dots]$ , where  $\mathbf{x}'(k-1) = [\mathbf{x}(k), 1]$ . The output is

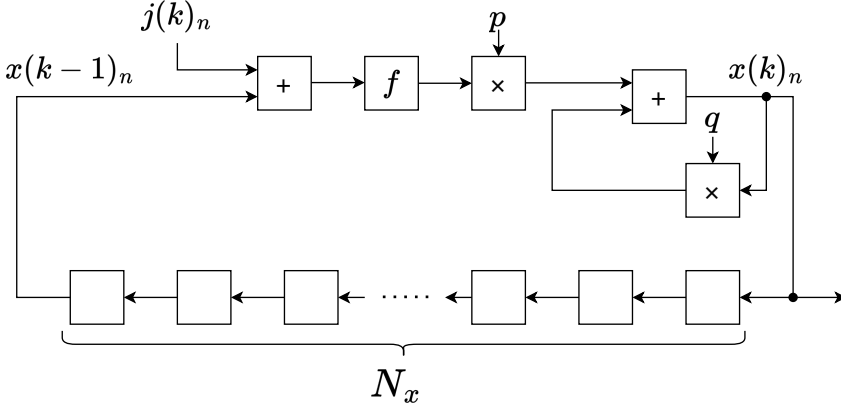


Fig. 3. Block diagram of reservoir processing in the modular DFR model. The block labeled “ $f$ ” operates as a one-input, one-output function  $f$  in Eq. (2). Only two parameters,  $p$  and  $q$ , have to be optimized.

obtained using the output layer  $W_{\text{out}}$ , where  $N_r$  represents the number of features in a reservoir representation:

$$\mathbf{y} = W_{\text{out}}\mathbf{r} + \mathbf{b} = \sum_{n=1}^{N_r} \mathbf{w}_n r_n + \mathbf{b}. \quad (13)$$

For each of the components of  $\mathbf{r}$ , multiple reservoir states are used in the derivation, making backpropagation complicated and challenging.

## 2.4 Modular DFR

The challenge in designing a DFR lies in determining the design of the NL. Existing analog implementations utilize elements that obey a delay differential equation, while digital implementations that approximate the behavior of analog NL elements.

The modular DFR presents a model that simplifies the design of the NL in the digital implementation of DFR [11]. To streamline the design process, the NL operation is decomposed into multiple blocks, replacing the delay differential equation with a one-input, one-output function  $f$ . This simplification also reduces the number of adjustable parameters while preserving the original solution space [11]. Fig. 3 illustrates the block diagram of the modular DFR model. Here,  $x(k)_n$  can be represented as follows:

$$x(k)_n = pf(j(k)_n + x(k-1)_n) + qx(k)_{n-1}. \quad (14)$$

In Eq. (14), the parameters to be optimized are  $p$  and  $q$ . Together with the regularization parameter used for linear regression in the output layer, a total of three parameters require optimization. However, even after reducing the number of parameters, grid search remains challenging due to the need to explore the three-dimensional parameter space. Suboptimal selection of these parameters can lead to insufficient accuracy. Thus, an efficient optimization strategy is crucial for effective parameter tuning.

## 2.5 Training of the output layer using Gaussian elimination

---

**Algorithm 1** Ridge regression using Gaussian elimination
 

---

**Input:**  $A[N_y][s]$ ,  $B[s][s]$ ,  $B^{-1}[s][s]$ ,  $buf$ 
**Output:**  $\tilde{W}_{out}[N_y][s]$ 

```

1: for  $i = 0$  to  $s - 1$  do
2:   for  $j = 0$  to  $s - 1$  do
3:     if  $i == j$  then
4:        $B^{-1}[i][j] \leftarrow 1$ 
5:     else
6:        $B^{-1}[i][j] \leftarrow 0$ 
7:     end if
8:   end for
9: end for
10: for  $i = 0$  to  $s - 1$  do
11:    $buf \leftarrow 1/B[i][i]$ 
12:   for  $j = 0$  to  $s - 1$  do
13:      $B[i][j] \leftarrow B[i][j] * buf$ 
14:      $B^{-1}[i][j] \leftarrow B^{-1}[i][j] * buf$ 
15:   end for
16:   for  $j = 0$  to  $s - 1$  do
17:     if  $i \neq j$  then
18:        $buf \leftarrow B[j][i]$ 
19:       for  $k = 0$  to  $s - 1$  do
20:          $B[j][k] \leftarrow B[j][k] - B[i][k] * buf$ 
21:          $B^{-1}[j][k] \leftarrow B^{-1}[j][k] - B^{-1}[i][k] * buf$ 
22:       end for
23:     end if
24:   end for
25: end for
26: for  $i = 0$  to  $N_y - 1$  do
27:   for  $j = 0$  to  $s - 1$  do
28:      $\tilde{W}_{out}[i][j] \leftarrow 0$ 
29:     for  $k = 0$  to  $s - 1$  do
30:        $\tilde{W}_{out}[i][j] \leftarrow \tilde{W}_{out}[i][j] + A[i][k] * B^{-1}[k][j]$ 
31:     end for
32:   end for
33: end for

```

---

The output layer of the DFR is typically trained using Ridge regression. The output  $\mathbf{y}$  and the target output  $\mathbf{e}$  are the following vectors:

$$\mathbf{y} = [y_1, y_2, \dots, y_{N_y}] \text{ and } \mathbf{e} = [e_1, e_2, \dots, e_{N_y}]. \quad (15)$$

Here,  $N_y$  represents the number of classes, and  $\mathbf{e}$  is represented using a one-hot encoding. We define the following:

$$\tilde{\mathbf{r}} \equiv [\mathbf{r}, 1]. \quad (16)$$

Eq. (13) is expressed as follows:

$$\mathbf{y} = \tilde{W}_{\text{out}} \tilde{\mathbf{r}}. \quad (17)$$

We subsequently define the following:

$$\tilde{R} \equiv [\tilde{\mathbf{r}}^1, \tilde{\mathbf{r}}^2, \dots, \tilde{\mathbf{r}}^{\text{Train}}] \text{ and } E \equiv [\mathbf{e}^1, \mathbf{e}^2, \dots, \mathbf{e}^{\text{Train}}], \quad (18)$$

where Train is the number of training data. In Ridge regression,  $\tilde{W}_{\text{out}}$  is derived as follows:

$$\tilde{W}_{\text{out}} = E \tilde{R}^T (\tilde{R} \tilde{R}^T + \beta I)^{-1}, \quad (19)$$

where  $I$  is an identity matrix and  $\beta$  is a regularization parameter. To simplify the following explanation, we define:

$$s \equiv N_x^2 + N_x + 1, \quad (20)$$

$$A \equiv E \tilde{R}^T \in \mathbb{R}^{N_y \times s}, \quad (21)$$

$$B \equiv \tilde{R} \tilde{R}^T + \beta I \in \mathbb{R}^{s \times s}. \quad (22)$$

Then, Eq. (19) is expressed as follows:

$$\tilde{W}_{\text{out}} = AB^{-1}. \quad (23)$$

Algorithm 1 shows a pseudo code to perform Ridge regression by computing the matrix inversion using Gaussian elimination [5]. Note that the array indexes start from zero, and that the first and second dimensions represent rows and columns, respectively.

### 3 ONLINE EDGE TRAINING AND INFERENCE SYSTEM OF DELAYED FEEDBACK RESERVOIR

#### 3.1 System overview

In this section, we propose an online edge training and inference system of DFR characterized by the following key features.

- Leveraging the modular DFR as its foundational structure, our system maintains task-specific extensibility of the NL. We propose backpropagation for reservoir parameter optimization, enabling tunable reservoir parameters that determine DFR accuracy. This approach significantly accelerates parameter optimization and reduces training time compared to conventional systems that rely on offline grid search. Special consideration are made for the DPRR and reservoir layers to facilitate backpropagation. The DPRR layer, having multiple roots for a single value, necessitates backpropagation from each root. Meanwhile, the recursive structure of the reservoir layer demands a considerable number of terms after expansion. To enable a more lightweight implementation, we propose a truncation approach to backpropagation.
- To minimize the memory footprint, we propose a new matrix manipulation technique based on Ridge regression in Eq. (23) for the output layer. The traditional Gaussian elimination methods for computing the inverse matrix demand substantial amount of memory, which can impede the edge implementation of output layer optimization. Instead, our approach employs in-place Cholesky decomposition, leveraging matrix symmetry to store approximately half the original matrix elements as a one-dimensional (1-D) array. This technique also enables memory sharing between the original matrix and intermediate calculations, further optimizing memory usage during matrix inversion and multiplication.

These new contributions enable the edge implementation of DFR for online training and inference, offering efficiency in terms of memory usage and runtime. The following subsections explain the backpropagation process in its natural order for error propagation, starting from the output layer, then moving to the DPRR layer and finally reaching the reservoir layer.

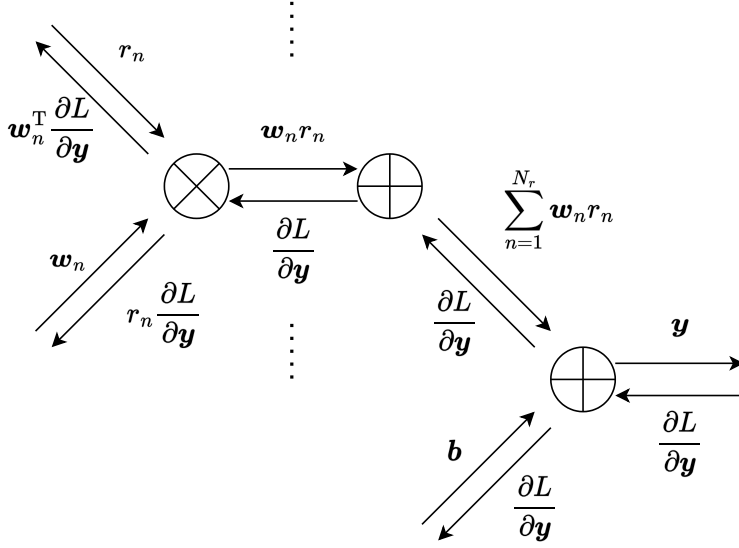


Fig. 4. Computation graph of forward and backward propagation in the output layer.

### 3.2 Backpropagation in the output layer

Fig. 4 illustrates the computation graph summarizing the backpropagation in the output layer. The loss function is formulated using cross entropy error as:

$$L = - \sum_{k=1}^{N_y} e_k \log y_k. \quad (24)$$

The partial derivative of  $L$  with respect to  $\mathbf{y}$  is given by:

$$\frac{\partial L}{\partial \mathbf{y}} = \mathbf{y} - \mathbf{e}, \quad (25)$$

which is propagated backwards through the network.

The computation in the output layer is expressed as Eq. (13). The partial derivatives of  $L$  with respect to  $\mathbf{b}$ ,  $\mathbf{r}_n$ , and  $\mathbf{w}_n$  are respectively expressed as follows:

$$\frac{\partial L}{\partial \mathbf{b}} = \frac{\partial L}{\partial \mathbf{y}}, \quad \frac{\partial L}{\partial \mathbf{r}_n} = \mathbf{w}_n^T \frac{\partial L}{\partial \mathbf{y}}, \quad \text{and} \quad \frac{\partial L}{\partial \mathbf{w}_n} = \mathbf{r}_n \frac{\partial L}{\partial \mathbf{y}}. \quad (26)$$

### 3.3 Backpropagation in the DPRR layer

Fig. 5 illustrates the computation graph summarizing the backpropagation in the DPRR layer. First, each feature in the DPRR is defined as follows:

$$r_{(i-1)N_x+j} = \sum_{k=1}^T x(k)_i x(k-1)_j \quad (i, j = 1, \dots, N_x), \quad (27)$$

$$r_{N_x^2+i} = \sum_{k=1}^T x(k)_i \quad (i = 1, \dots, N_x). \quad (28)$$

Errors are backpropagated from multiple reservoir representations for a feature  $x(k)_n$ , and the sum is backpropagated to the upstream layer. The following backpropagated value (bpv) is propagated

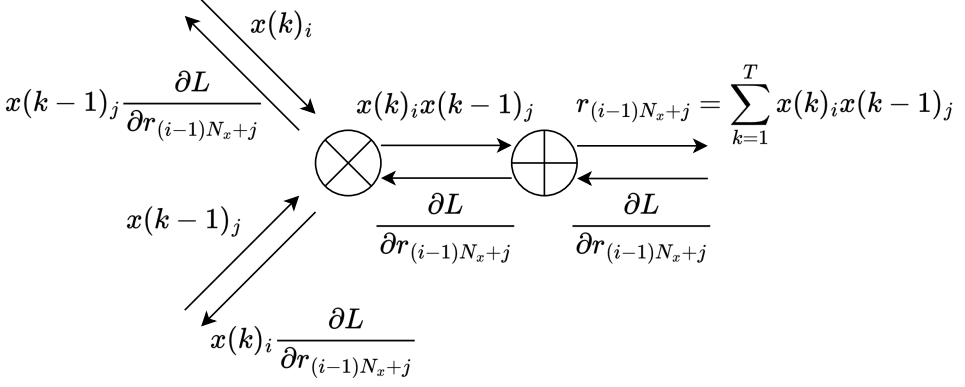


Fig. 5. Computation graph of forward and backward propagation in the DPRR layer.

from the DPRR layer for the partial derivative of  $L$  with respect to  $x(k)_n$ .

$$\begin{aligned}
 (\text{bpv}) = & \sum_{j=1}^{N_x} x(k-1)_j \frac{\partial L}{\partial r_{(n-1)N_x+j}} \\
 & + \sum_{i=1}^{N_x} x(k+1)_i \frac{\partial L}{\partial r_{(i-1)N_x+n}} + \frac{\partial L}{\partial r_{N_x^2+n}}.
 \end{aligned} \quad (29)$$

### 3.4 Backpropagation in the reservoir layer

Fig. 6 illustrates the computation graph summarizing the backpropagation in the reservoir layer. Unfolding the recurrent structure of the reservoir using the modular DFR model, the sum of errors

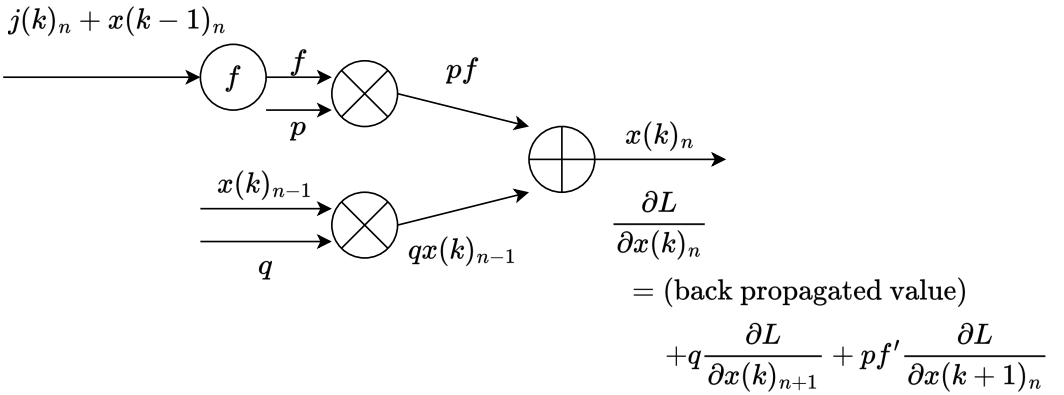


Fig. 6. Computation graph of forward and backward propagation in the reservoir layer.

from different nodes and different times, and errors propagated from the downstream DPRR layer

are backpropagated. The partial derivative of  $L$  with respect to  $x(k)_n$  is recursively given as:

$$\frac{\partial L}{\partial x(k)_n} = (\text{bpv}) + q \frac{\partial L}{\partial x(k)_{n+1}} + p f' \frac{\partial L}{\partial x(k+1)_n}. \quad (30)$$

The partial derivative of  $L$  with respect to the constant multiplication parameters  $p$  and  $q$  are respectively given by summing up for all past times as follows:

$$\frac{\partial L}{\partial p} = \sum_{k=1}^T f(j(k)_n + x(k-1)_n) \frac{\partial L}{\partial x(k)_n}, \quad (31)$$

$$\frac{\partial L}{\partial q} = \sum_{k=1}^T x(k)_{n-1} \frac{\partial L}{\partial x(k)_n}. \quad (32)$$

### 3.5 Truncated Backpropagation

For (bpv) in Eq. (29), the value of  $\frac{\partial L}{\partial r}$  is determined at time  $T$ . This means that the reservoir state must be stored for the number of times used for backpropagation plus one time. Therefore, to use the entire time series,  $(T+1)$  reservoir states must be stored, which consumes quadratically larger memory space as  $T$  increases. To alleviate the memory usage while maintaining optimization accuracy, we propose a *truncated backpropagation* method that uses only a limited number of reservoir states. For instance, only the last time is used. This approximation is based on the property that the last reservoir state encompasses past reservoir states cumulatively, with the impact of past states gradually diminishing. With this approximation, Eqs. (29),(30),(31), and (32) are respectively simplified as follows:

$$(\text{bpv}) = \sum_{j=1}^{N_x} x(T-1)_j \frac{\partial L}{\partial r_{(n-1)N_x+j}} + \frac{\partial L}{\partial r_{N_x^2+n}}, \quad (33)$$

$$\frac{\partial L}{\partial x(T)_n} = (\text{bpv}) + q \frac{\partial L}{\partial x(T)_{n+1}}, \quad (34)$$

$$\frac{\partial L}{\partial p} = f(j(T)_n + x(T-1)_n) \frac{\partial L}{\partial x(T)_n}, \quad (35)$$

$$\frac{\partial L}{\partial q} = x(T)_{n-1} \frac{\partial L}{\partial x(T)_n}. \quad (36)$$

By comparing Eqs. (31) and (32) with Eqs. (35) and (36), it becomes evident that the computational effort is significantly reduced by approximately  $1/T$ . This simplification allows us to store only two reservoir states:  $x(T-1)$  and  $x(T)$ . Specifically, for datasets with a time series length  $T$  greater than 100, which holds true for most datasets, the memory requirement for the reservoir state can be reduced to less than 2% of the original. When considering overall memory usage for solving a three-class classification task with a time series length of  $T = 500$  and  $N_x = 30$ , memory usage can be reduced by approximately 80%, including other weights such as output weights.

### 3.6 In-place Ridge Regression via 1-D Cholesky Decomposition

The method proposed in the previous section enables hitherto offline parameter search for DFR to online execution. In addition, edge devices require learning and implementing the output layer with minimal memory footprint. In this section, we propose in-place Ridge regression via 1-D Cholesky decomposition.

In calculating Eq. (23), matrix  $B$  is symmetric because it is expressed as follows:

$$B = (\tilde{\mathbf{r}}^1 \dots \tilde{\mathbf{r}}^{\text{Train}}) \begin{pmatrix} \tilde{\mathbf{r}}^1 \text{ }^T \\ \dots \\ \tilde{\mathbf{r}}^{\text{Train}} \text{ }^T \end{pmatrix} + \beta I, \quad (37)$$

$$= \sum_{k=1}^{\text{Train}} \tilde{\mathbf{r}}^k \tilde{\mathbf{r}}^k \text{ }^T + \beta I. \quad (38)$$

For any nonzero real vectors  $\mathbf{z}$ ,  $\mathbf{r}\mathbf{r}^T$  is positive definite:

$$\mathbf{z}^T (\tilde{\mathbf{r}}\tilde{\mathbf{r}}^T) \mathbf{z} = \langle \mathbf{z}, \tilde{\mathbf{r}} \rangle \langle \tilde{\mathbf{r}}, \mathbf{z} \rangle > 0. \quad (39)$$

Therefore,  $B$  is also positive definite because it is derived as the sum of positive definite matrices. Consequently,  $B$  can be decomposed using Cholesky decomposition into the lower triangular matrix  $C$ :

$$B = CC^T. \quad (40)$$

Since matrix  $B$  is symmetric, it suffices to store only the lower triangular components. Additionally, by optimizing the order of decomposition computation, matrix  $C$  can be derived in-place, i.e., matrices  $C$  and  $B$  can share the same memory space during decomposition requiring no additional memory. This reduction is significant because the number of elements in  $B$  is proportional to the fourth power of  $N_x$ .

We will perform the proposed Cholesky decomposition using a 1-D array  $P$  of size  $s(s+1)/2$ , to facilitate hardware implementation. The matrix  $P$  initially stores the components of  $B$ :

$$P[i(i+1)/2 + j] = B[i][j]. \quad (41)$$

The components of the lower triangle are stored sequentially in the row direction. Similarly, the decomposed matrix is stored according to Algorithm 2:

$$P[i(i+1)/2 + j] \leftarrow C[i][j]. \quad (42)$$

Algorithm 2 provides a pseudo code for the proposed in-place Cholesky decomposition. First,  $C[0][0]$  is obtained as  $C[0][0] = \sqrt{B[0][0]}$  (line 5, with  $i = 0$ ) and  $C[X][0]$  is calculated by  $C[X][0] = B[X][0]/C[0][0]$ , where  $X = 1, \dots, s-1$  (line 10). Next,  $C[1][1]$  is obtained as  $C[1][1] = \sqrt{B[1][1] - C[1][0]^2}$  (lines 2–5, with  $i = 1$ ) and  $C[X][1]$  is calculated by  $C[X][1] = (B[X][1] - C[X][0]C[1][0])/C[1][1]$ , where  $X = 2, \dots, s-1$  (lines 7–12, with  $i = 1$ ). Similarly, the remaining elements can be calculated by first determining the diagonal element, and then computing the off-diagonals sequentially. It is important to note the variable dependence in these computations—to compute each left-hand side component, all components appearing in the right-hand side are stored in the array  $P$ , necessitating no additional memory space other than a few registers.

Using Eqs. (23) and (40),  $A$  is expressed as:

$$A = (\tilde{W}_{\text{out}} C) C^T = D C^T, \quad (43)$$

where  $D \equiv \tilde{W}_{\text{out}} C$ . We will first compute  $D$  and then  $\tilde{W}_{\text{out}}$  both in-place using the fact that  $C$  is triangular.

Algorithm 3 shows a pseudo code to compute  $D = A(C^T)^{-1}$  using backward substitution. First,  $D[0][0]$  is calculated by  $D[0][0] = A[0][0]/C[0][0]$  (line 6, with  $(i, j) = (0, 0)$ ) and then  $D[0][1]$  is calculated by  $D[0][1] = (A[0][1] - D[0][0]C[1][0])/C[1][1]$  (lines 3–6, with  $(i, j) = (0, 1)$ ) and  $D[0][Y]$ , where  $Y = 2, \dots, s-1$ , can be calculated sequentially. For the other rows, the values are calculated from the left column. Once again, this calculation is conducted entirely in-place because all components appearing in the right-hand side for the same row exist in  $A$  and  $Q$ . Each element in  $A$  is used only once, enabling the storage space to be shared with the output.

---

**Algorithm 2** Cholesky decomposition in 1-D array
 

---

**Input:**  $P[s(s+1)/2]$  storing  $B$ **Input:**  $buf$ **Ensure:**  $P[s(s+1)/2]$  storing  $C$ 

```

1: for  $i = 0$  to  $s - 1$  do
2:   for  $j = 0$  to  $i - 1$  do
3:      $P[i(i+1)/2 + i] \leftarrow P[i(i+1)/2 + i] - P[i(i+1)/2 + j] * P[i(i+1)/2 + j]$ 
4:   end for
5:    $P[i(i+1)/2 + i] \leftarrow \text{sqrt}(P[i(i+1)/2 + i])$ 
6:    $buf \leftarrow 1/P[i(i+1)/2 + i]$ 
7:   for  $j = i + 1$  to  $s - 1$  do
8:     for  $k = 0$  to  $i - 1$  do
9:        $P[j(j+1)/2 + i] \leftarrow P[j(j+1)/2 + i] - P[i(i+1)/2 + k] * P[j(j+1)/2 + k]$ 
10:    end for
11:     $P[j(j+1)/2 + i] \leftarrow P[j(j+1)/2 + i] * buf$ 
12:  end for
13: end for

```

---



---

**Algorithm 3** Calculation of  $\tilde{W}_{\text{out}}C$ 


---

**Input:**  $Q[N_y][s]$  storing  $A$ **Input:**  $P[s(s+1)/2]$  storing  $C$ **Ensure:**  $Q[N_y][s]$  storing  $D$ 

```

1: for  $i = 0$  to  $N_y - 1$  do
2:   for  $j = 0$  to  $s - 1$  do
3:     for  $k = 0$  to  $j - 1$  do
4:        $Q[i][j] \leftarrow Q[i][j] - Q[i][k] * P[j(j+1)/2 + k]$ 
5:     end for
6:      $Q[i][j] \leftarrow Q[i][j] / P[j(j+1)/2 + j]$ 
7:   end for
8: end for

```

---

In a similar manner, we solve  $\tilde{W}_{\text{out}} = DC^{-1}$  through the in-place forward substitution utilizing the fact that  $C$  is a lower triangular matrix. Algorithm 4 presents pseudo code for the computation of  $\tilde{W}_{\text{out}}$ . The calculation starts with  $\tilde{W}_{\text{out}}[0][n-1] = D[0][n-1]/C[n-1][n-1]$  (line 6, with  $(i, j) = (0, n-1)$ ). Next,  $\tilde{W}_{\text{out}}[0][n-2]$  is calculated by  $\tilde{W}_{\text{out}}[0][n-2] = (D[0][n-2] - \tilde{W}_{\text{out}}[0][n-1])$  (lines 3–6, with  $(i, j) = (0, n-2)$ ) and  $\tilde{W}_{\text{out}}[0][Y]$ , where  $Y = n-3, \dots, 0$ , can be similarly calculated sequentially. For the other rows, the values are calculated from the right column.

Table 2 summarizes memory consumption in data words, which is the matrix element values, typically as 32-bit floating point numbers. If  $N_y$  is sufficiently small compared to  $s$ , the proposed method reduces memory consumption to approximately one-fourth of that required by the conventional Gaussian elimination method. Table 3 compares the number of arithmetic operations. Under similar conditions, when  $N_y$  is sufficiently small compared to  $s$ , the proposed method reduces the

**Algorithm 4** Calculation of  $\tilde{W}_{\text{out}}$ **Input:**  $Q[N_y][s]$  storing  $D$ **Input:**  $P[s(s+1)/2]$  storing  $C$ **Ensure:**  $Q[N_y][n]$  storing  $\tilde{W}_{\text{out}}$ 

```

1: for  $i = 0$  to  $N_y - 1$  do
2:   for  $j = s - 1$  to  $0$  do
3:     for  $k = s - 1$  to  $j + 1$  do
4:        $Q[i][j] \leftarrow Q[i][j] - Q[i][k] * P[k(k+1)/2 + j]$ 
5:     end for
6:      $Q[i][j] \leftarrow Q[i][j] / P[j(j+1)/2 + j]$ 
7:   end for
8: end for

```

Table 2. Memory footprint. “Naive” and “Proposed” represent the calculation via Gaussian elimination and 1-D Cholesky decomposition, respectively.

	naive	proposed
memory [word]	$2s(s + N_y) + 1$	$\frac{1}{2}s(s + 2N_y) + \frac{1}{2}s$

Table 3. Number of arithmetic operations. “Naive” and “Proposed” represent the calculation via Gaussian elimination and 1-D Cholesky decomposition, respectively.

op.	naive	proposed
add	$2s^2(s + \frac{1}{2}N_y) - 2s^2$	$\frac{1}{6}s^2(s + N_y) - \frac{1}{6}s - sN_y$
mul	$2s^2(s + \frac{1}{2}N_y)$	$\frac{1}{6}s^2(s + N_y) + \frac{1}{2}s^2 - \frac{2}{3}s - sN_y$
div	$s$	$s + 2sN_y$
sqrt	$0$	$s$

number of additions and multiplications to about one-twelfth of those required by the Gaussian elimination method.

## 4 EVALUATION

In this section, we evaluate the fast reservoir parameter optimization method, the memory-saving Ridge regression, and the online edge training and inference system achieved by combining them. The evaluation uses the same datasets (npz files) as in [6]. Table 4 provides a summary of the datasets used. The evaluations consistently used  $f(x) = \alpha x$  as the nonlinear function in the modular DFR for all datasets, as recommended in [11]. The reservoir size  $N_x$  was set to 30.

### 4.1 Evaluation of the proposed fast parameter optimization for the reservoir layer

The proposed parameter optimization method was evaluated on a Windows workstation equipped with an AMD Ryzen 7 5825U CPU and 16 GB of memory. All programs were implemented in Python 3.9.6 and utilized the numpy library version 1.23.0.

Table 4. Summary of multivariate time series classification datasets (taken from [6]). Column #V, #C, Train, and Test respectively report the input dimension, the output dimension, the number of training data, and that of testing data.  $T_{\min}$  and  $T_{\max}$  are the shortest and the longest length of the input series in the dataset, respectively.

Dataset	#V	#C	Train	Test	$T_{\min}$	$T_{\max}$
ARAB	13	10	6600	2200	4	93
AUS	22	95	1140	1425	45	136
CHAR	3	20	300	2558	109	205
CMU	62	2	29	29	127	580
ECG	2	2	100	100	39	152
JPVOW	12	9	270	370	7	29
KICK	62	2	16	10	274	841
LIB	2	15	180	180	45	45
NET	4	13	803	534	50	994
UWAV	3	8	200	427	315	315
WAF	6	2	298	896	104	198
WALK	62	2	28	16	128	1918

In the proposed method, the reservoir parameters  $p$  and  $q$ , along with the output-layer parameters  $W_{\text{out}}$  and  $b$  are optimized using the proposed truncated backpropagation. The initial values of  $[p, q]$  are  $[0.01, 0.01]$ , and the output parameters are initialized to zeros. The stochastic gradient descent is employed for 25 epochs. The learning rate started at 1 and was reduced by multiplying 0.1 for the reservoir layer parameters at epochs 5, 10, 15, and 20. For the output layer parameters, the learning rate was multiplied by 0.1 at epochs 10, 15, and 20. Once the optimization with backpropagation is completed, the output layer is trained using Ridge regression with the regularization parameter  $\beta$ . We evaluate  $\beta$  values of  $[10^{-6}, 10^{-4}, 10^{-2}, 10^0]$  and choose the one resulting in the lowest loss  $L$ .

We compared the proposed method with grid search, which was executed in three dimensions:  $p$ ,  $q$ , and  $\beta$ . The ranges for  $p$  and  $q$  were set to  $[10^{-3.75}, 10^{-0.25}]$ ,  $[10^{-2.75}, 10^{-0.25}]$ , respectively. These ranges were determined to cover the optimal parameters for all the datasets used in this evaluation. The number of grid divisions is increased from 1 until the accuracy matches that of the proposed method. Note that the grid divisions are equidistant, e.g., the range for  $p$  and  $q$  are simultaneously divided into sections of equal length.  $\beta$  is searched in the same way as the proposed method.

Table 5 summarizes the comparison results for accuracy and computation time. The parameters optimized with backpropagation attained equal or superior accuracy to the state-of-the-art [10] for most datasets, while significantly reducing the computation time to approximately 1/700 of that of the grid search.

Fig. 7 compares the parameter optimization times between the proposed method and grid search. The results demonstrate that the proposed method not only achieves superior accuracy—closer to the true optimal parameters—but also reduces computation time by several orders of magnitude. The reduction in computation time is particularly significant for datasets where grid search requires a long computation time. For datasets requiring fewer grid divisions indicate either the optimal parameters are widely spread, or that the initial coarse grid coincidentally yields satisfactory outcomes. However, the practical challenges of grid search include the difficulty of determining whether the best accuracy has been attained, making early stopping unreliable. In contrast, datasets with sharp and narrowly defined optimal parameters necessitate very fine grid divisions for accurate optimization. In such cases, grid search may demand exponentially long computation time.

Table 5. Runtime comparison between the proposed backpropagation (bp) and grid search (gs). Column “gs divs” represents the number of grid divisions required to achieve equal accuracy as the proposed method (bp acc).

dataset	bp acc	bp time (s)	gs divs	gs time (s)	(gs time)/ (bp time)
ARAB	0.981	245	8	25,040	102.2
AUS	0.954	54	8	5,535	102.5
CHAR	0.918	44	10	4,820	109.5
CMU	0.931	4	1	3	0.8
ECG	0.850	11	16	4,977	452.5
JPVOW	0.978	4	4	106	26.5
KICK	0.800	7	1	2	0.3
LIB	0.806	12	18	8,423	701.9
NET	0.783	45	1	49	1.1
UWAV	0.850	65	10	6,322	97.3
WAF	0.983	14	3	188	13.4
WALK	1.000	4	1	3	0.8

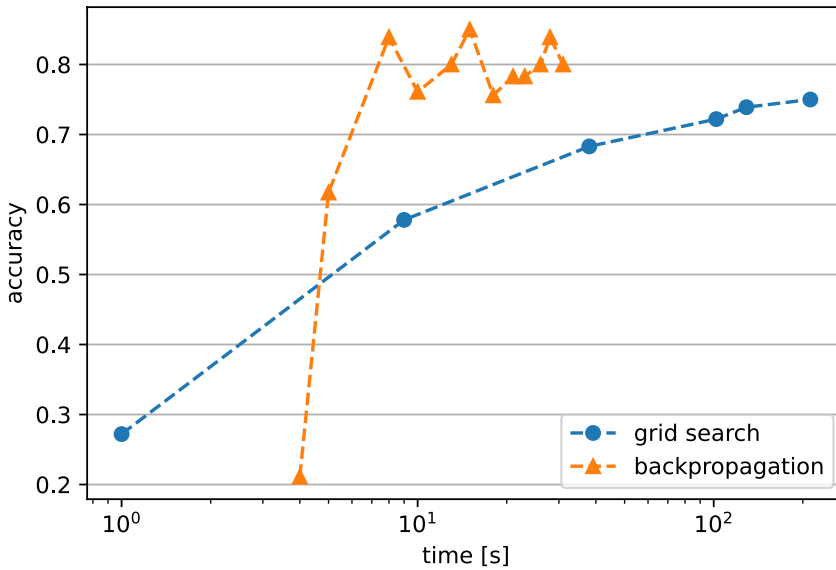


Fig. 7. Accuracy versus computation time for the dataset LIB.

Table 6 compares classification accuracy with other machine learning methods. The machine learning methods that were compared were:

- (1) Multi layer perceptron (MLP) [23]
- (2) Fully convolutional neural network (FCN) [23]
- (3) Residual network (ResNet) [23]
- (4) Encoder [18]
- (5) Multi channel deep convolutional neural network (MCDCNN) [25]

Table 6. Classification accuracy comparison with other machine learning methods. The data in the table, except for prop. bp, are from [12].

dataset	MLP	FCN	ResNet	Encoder	MDCNN	Time-ECN	TWIESN	prop. bp
ARAB	0.969	0.994	0.996	0.981	0.959	0.958	0.853	0.981
AUS	0.933	0.975	0.974	0.938	0.854	0.726	0.724	0.954
CHAR	0.969	0.990	0.990	0.971	0.938	0.960	0.920	0.918
CMU	0.600	1.000	0.997	0.983	0.514	0.976	0.893	0.931
ECG	0.748	0.872	0.867	0.872	0.500	0.841	0.737	0.850
JPVOW	0.976	0.993	0.992	0.976	0.944	0.956	0.965	0.978
KICK	0.610	0.540	0.510	0.610	0.560	0.620	0.670	0.800
LIB	0.780	0.964	0.954	0.783	0.651	0.637	0.794	0.806
NET	0.550	0.891	0.627	0.777	0.630	0.890	0.945	0.783
UWAV	0.901	0.934	0.926	0.908	0.845	0.859	0.754	0.850
WAF	0.894	0.982	0.989	0.986	0.658	0.948	0.949	0.983
WALK	0.700	1.000	1.000	1.000	0.450	1.000	0.944	1.000

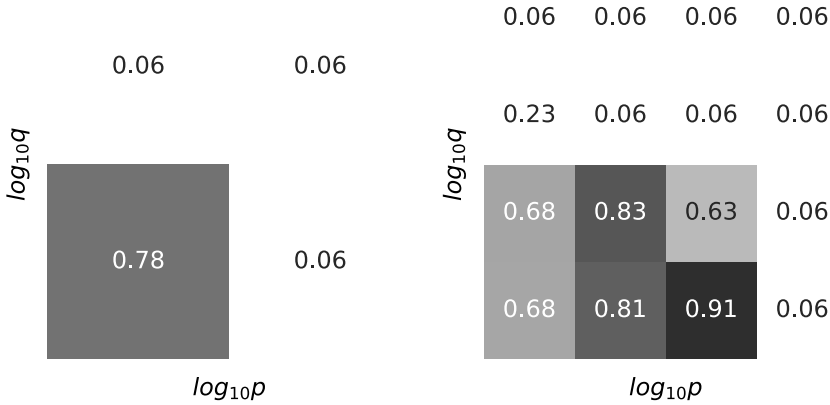


Fig. 8. Grid search example where recursively subdividing the previously best grid is challenging. The dataset used is CHAR. Left: grid level 1, right: grid level 2.

(6) Time convolutional neural network (Time-CNN) [24]

(7) Time warping invariant echo state network (TWIESN). [22]

The proposed backpropagation method (prop. bp) achieves an accuracy better than or comparable to all these machine learning methods.

An alternative approach to explore a finer parameter space is to recursively divide the best region in the coarser search. However, this method may result in suboptimal parameters and fail for certain datasets if the coarse grid search does not yield globally optimal parameters, as illustrated in Fig. 8. The proposed method successfully identified optimal values with a fixed number of epochs for all datasets used in this study. Although exploring different initial values or increasing epochs could potentially lead to further improvements, they did not enhance the accuracy of the presented datasets.

Table 7 shows the memory savings resulting from the truncation of the backpropagation calculations. While the reduction in memory is relatively smaller for datasets with a large number of

Table 7. Storage reduction by truncated backpropagation. “Naive” and “simplified” represent the total number of stored values of the reservoir state, reservoir representation, and reservoir weight, before and after truncating the computation of backpropagation. The datapath is consistently calculated by a word, which is float32.

dataset	naive [word]	simplified [word]	(naive-simplified)/ naive
ARAB	13,030	10,300	21 %
AUS	93,455	89,435	4 %
CHAR	25,700	19,610	24 %
CMU	20,192	2,852	86 %
ECG	7,352	2,852	61 %
JPVOW	10,179	9,369	8 %
KICK	28,022	2,852	90 %
LIB	16,245	14,955	8 %
NET	42,853	13,093	69 %
UWAV	17,828	8,438	53 %
WAF	8,732	2,852	67 %
WALK	60,332	2,852	95 %

classes and short input series lengths, more than half of the datasets still achieve a reduction of over 50%. In addition, for all datasets, even those with small memory reductions, the computational effort of backpropagation has been reduced to approximately  $1/T$ , resulting in a considerable reduction in computation time.

#### 4.2 Evaluation of the proposed memory-saving Ridge regression for the output layer

Next, we evaluate the proposed in-place Ridge regression via 1-D Cholesky Decomposition. The evaluation environment remains unchanged from Section 4.1. The optimal parameters obtained by the proposed parameter optimization in Section 4.1 are used to perform Ridge regression. The naive method with Gaussian elimination and the proposed method with 1-D Cholesky decomposition are compared.

Fig. 9 plots the ratio of computation times between Gaussian elimination and proposed Cholesky decomposition. Lighter shades represent faster computation times achieved by the proposed method relative to the Gaussian elimination. The proposed method demonstrates consistent and significant speed advantages for practical  $N_x$  values exceeding 10. Notably, for  $N_y$  values below 10, the proposed method achieves a speedup of approximately 7x. While the proposed method introduces additional division and square root operations, the substantial reduction in the number of additions and multiplications significantly reduces the total computation time.

Table 8 shows the memory savings achieved by using the proposed Ridge regression. Despite achieving the same accuracy as the naive method, the proposed method reduces memory usage by almost four times for all datasets.

#### 4.3 Hardware implementation

The proposed parameter optimization method and Ridge regression were used to implement an on-line edge training and inference system of DFR on an FPGA board using Zynq-7000 (xc7z020clg400-1). The C++ code was synthesized in Xilinx Vitis HLS 2021.1, and the circuit was implemented and evaluated in Xilinx Vivado 2021.1. Although this paper demonstrates limited synthetic examples,

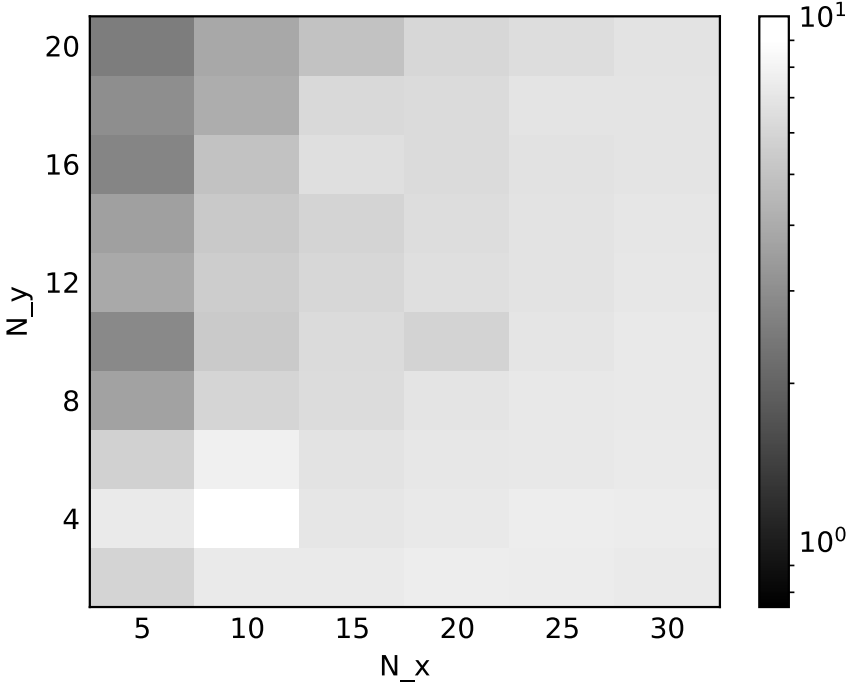


Fig. 9. Runtime ratio of the calculation via Gaussian elimination to via Cholesky decomposition.

Table 8. Memory usage in Ridge regression. “Naive” and “Prop.” use Gaussian elimination and Cholesky decomposition, respectively. A 32-bit float is evaluated as one word.

data set	accuracy		memory [word]]		(naive mem)/ (prop. mem)
	naive	prop.	naive	prop.	
ARAB	0.981	0.981	1,752,142	443,156	3.95
AUS	0.954	0.954	1,910,412	522,291	3.66
CHAR	0.918	0.918	1,770,762	452,466	3.91
CMU	0.931	0.931	1,737,246	435,708	3.99
ECG	0.850	0.850	1,737,246	435,708	3.99
JPVOW	0.978	0.978	1,750,280	442,225	3.96
KICK	0.800	0.800	1,737,246	435,708	3.99
LIB	0.806	0.806	1,761,452	447,811	3.93
NET	0.783	0.783	1,757,728	445,949	3.94
UWAV	0.850	0.850	1,748,418	441,294	3.96
WAF	0.983	0.983	1,737,246	435,708	3.99
WALK	1.000	1.000	1,737,246	435,708	3.99

HLS enables flexible adjustments to trade-off between power and resource consumption, making it especially suitable for edge computing applications.

The hardware implementation was relatively straightforward owing to the design of the proposed algorithms. However, bottlenecks were identified in the computation of reservoir representations,

**Algorithm 5** Improved calculation of  $\tilde{W}_{\text{out}}C$ 


---

**Input:**  $Q[N_y][s]$  storing  $A$   
**Input:**  $P[s(s+1)/2]$  storing  $C$   
**Input:**  $\text{reg}[\text{RegSize} + 1]$   
**Ensure:**  $Q[N_y][s]$  storing  $D$

```

1: for  $i = 0$  to  $N_y - 1$  do
2:   for  $j = 0$  to  $s - 1$  do
3:     for  $k = 0$  to  $j - 1$  do
4:        $\text{mul} \leftarrow Q[i][k] * P[j(j+1)/2 + k]$ 
5:        $\text{idx} \leftarrow 0$ 
6:       for  $l = 0$  to  $\text{RegSize} - 1$  do
7:         if  $l == 0$  then
8:           if  $\text{idx} < \text{RegSize}$  then
9:              $\text{reg}[\text{RegSize}] \leftarrow -\text{mul}$ 
10:          else
11:             $\text{reg}[\text{RegSize}] \leftarrow \text{reg}[0] - \text{mul}$ 
12:          end if
13:        end if
14:         $\text{reg}[l] \leftarrow \text{reg}[l + 1]$ 
15:      end for
16:       $\text{idx} \leftarrow \text{idx} + 1$ 
17:    end for
18:    for  $k = 0$  to  $\text{RegSize}$  do
19:       $Q[i][j] \leftarrow Q[i][j] - \text{reg}[k]$ 
20:    end for
21:     $Q[i][j] \leftarrow Q[i][j] / P[j(j+1)/2 + j]$ 
22:  end for
23: end for

```

---

backpropagation, and ridge regression. To address these challenges, loops within these processes were carefully pipelined. In particular, memory dependencies arising from successive accesses to the same address locations, as shown in line 4 of Algorithm 3, constrained the reduction of iteration intervals. To mitigate this limitation, small write buffers were introduced. Consequently, Algorithm 3 was revised into Algorithm 5, where  $Q$  was partitioned to enable parallelism. Similar optimization was applied to Algorithm 4.

Fig. 10 illustrates the effectiveness of incorporating the write buffer. In the naive implementation, multiplication and subtraction operations followed by memory writes had to complete within a single clock period, significantly limiting the achievable clock frequency. In contrast, the improved implementation allows these operations to finish before the subsequent loop iteration after all write buffers are filled. This buffer significantly relaxes timing constraints and enabling pipelining at the cost of increased DSP usage. The value of  $\text{RegSize}$  was carefully determined to balance trade-offs. A larger  $\text{RegSize}$  allows for greater parallel processing in lines 3–17 of Algorithm 5, but it also increases loop iterations in lines 18–20 and introduces memory access conflicts. After balancing these considerations, the value of  $\text{RegSize}$  was set to 4 throughout this work.

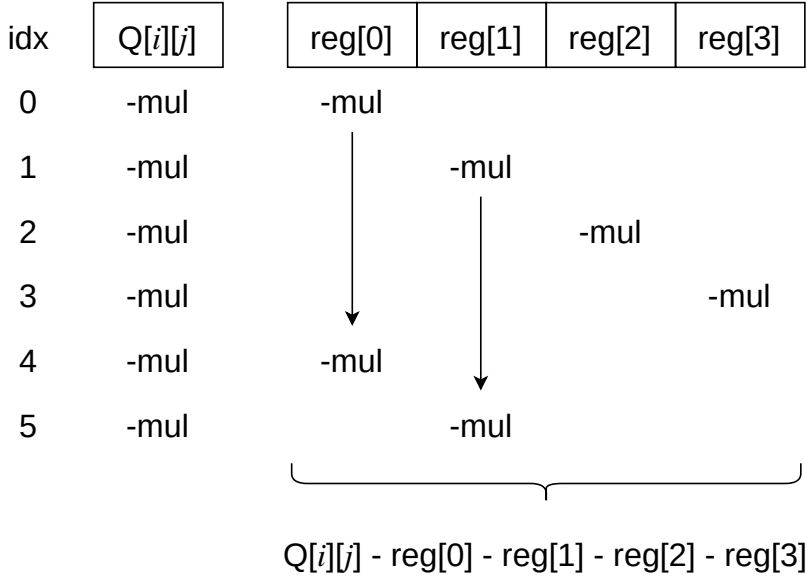


Fig. 10. Conceptual timing diagram showing the efficacy of adding a small write buffer.

Initially, prior to applying these optimizations, bottlenecks were identified in three key modules: reservoir representation, back propagation, and ridge regression. Among these, ridge regression posed the most significant bottleneck due to deeply nested memory-conflicting loops. The proposed optimizations resolved these conflicts, eliminating the bottleneck in ridge regression and shifting it to the reservoir state update, represented by Eqs. (8) and (9), which now determines the maximum achievable clock frequency.

To evaluate performance, a comparison was conducted between two implementation approaches: executing the entire process on the FPGA (HW-only) and running the corresponding C++ code using the processor on the same evaluation board (SW-only). The JPVOW dataset was used for the following evaluations.

Table 9 compares the implementation results. In hardware resource utilization, numbers in parentheses indicate the percentage of available FPGA resources used. The BRAM size is 36 kb per block. Power consumption was estimated using the Vivado tool after the place and route process, and the “Calculation time” represents the combined duration of training and inference executed sequentially. While the accuracy achieved by the software and hardware implementations is identical, the hardware implementation operates at a significantly lower maximum clock frequency compared to the Dual-core ARM Cortex-A9 MPCore processor on the FPGA board. Despite this, the hardware implementation reduced computation time to approximately 1/13 and power consumption to about 1/27. These results demonstrate the suitability of the proposed DFR system for execution on edge-hardware. Table 10 details resource utilization for each major module. Here, the DFR core module is responsible for processing the signal as it passes through the input, reservoir, and output layers. Note that these values were estimated after HLS and do not account for the resources used during the place and route process.

Table 11 presents synthesis results under different constraints, comparing non-pipelined and inlined configurations. The non-pipelined configuration was intended to minimize circuit size without incorporating pipelining, while the inlined configuration expanded the reservoir state

Table 9. Performance comparison between fully hardware (FPGA) and fully software implementations

	SW only	HW only
LUT	-	33,674 (63.2%)
LUTRAM	-	1,073 (6.2%)
FF	-	49,596 (46.6%)
BRAM	-	26.50 (18.9%)
DSP	-	143 (65.0%)
BUFG	-	1 (3.1%)
Clock frequency	667 MHz	100 MHz
FPGA power consumption	-	0.734 W
Processor power consumption	1.530 W	-
Calculation time	5.56 s	0.42 s
Training time	5.42 s	0.32 s
Inference time	0.14 s	0.10 s
Energy consumption	8.51 J	0.31 J

Table 10. Resource utilization of major modules

	DFR core	backpropagation	ridge regression
LUT	8,764	12,245	7,827
FF	11,266	10,125	8,228
DSP	15	57	20

Table 11. Performance comparison of non-pipelined and inlined configurations

	non-pipelined	inlined
LUT	22,680 (42.6%)	44,237 (83.2%)
LUTRAM	755 (4.3%)	884 (5.1%)
FF	31,953 (30.0%)	59,726 (56.13%)
BRAM	25.50 (18.2%)	27.50 (19.64%)
DSP	121 (55.0%)	136 (61.82 %)
BUFG	1 (3.1%)	1 (3.1%)
Clock frequency	100 MHz	100 MHz
FPGA power consumption	0.704 W	0.864 W
Calculation time	1.44 s	0.38 s
Training time	1.36 s	0.29 s
Inference time	0.09 s	0.09 s
Energy consumption	1.01 J	0.33 J

update process inline, addressing a bottleneck in the standard implementation. These results illustrate the Pareto front of the implementations, highlighting the flexibility offered by HLS for adopting various scenarios typical in edge computing environments.

Table 12 compares the proposed FPGA implementation of DFR with existing approaches. Unlike previous methods, which are limited to low-dimensional input-output tasks that are relatively simple

Table 12. Comparison with existing FPGA implementations of DFR. Columns #V and #C respectively report the input and output dimensions.

method	training/inference on HW	implementation	#V	#C
prop.	both	fully digital	12	9
[1]	inference only	fully digital	1	3
[19]	inference only	digital/analog hybrid	1	1

to implement, the proposed method supports practical and effective applications by performing both training and inference for multidimensional input-output tasks directly and entirely on the FPGA.

## 5 CONCLUSION

We proposed an online edge training and inference system for DFR, introducing several key innovations. First, we proposed a fast and accurate parameter optimization method for the reservoir layer using backpropagation and gradient descent. By adopting the modular DFR model, we formulated backpropagation for DPRR, enhancing accuracy while addressing computational challenges caused by long state dependencies. Additionally, a truncated backpropagation method was introduced, leveraging reservoir state properties to reduce computation time by up to approximately 1/700 and halve memory usage for most datasets. For the output layer, We proposed an in-place Ridge regression based on 1-D Cholesky decomposition. By utilizing matrix symmetry and optimizing the array update order, this method reduced memory usage by approximately 75% while maintaining accuracy. Finally, we implemented the entire system on an FPGA, incorporating these methods. The hardware implementation achieved an 13x reduction in computation time and a 27x reduction in power consumption simultaneously, compared to the software implementation on a dual-core ARM Cortex-A9 processor.

## REFERENCES

- [1] Miquel L Alomar, Miguel C Soriano, Miguel Escalona-Morán, Vincent Canals, Ingo Fischer, Claudio R Mirasso, and Jose L Rosselló. 2015. Digital implementation of a single dynamical node reservoir computer. *IEEE Transactions on Circuits and Systems II: Express Briefs* 62, 10 (2015), 977–981.
- [2] Shunichi Amari. 1993. Backpropagation and stochastic gradient descent method. *Neurocomputing* 5, 4-5 (1993), 185–196.
- [3] Lennert Appeltant, Miguel Cornelles Soriano, Guy Van der Sande, Jan Danckaert, Serge Massar, Joni Dambre, Benjamin Schrauwen, Claudio R Mirasso, and Ingo Fischer. 2011. Information processing using a single dynamical node as complex system. *Nature Communications* 2, 1 (2011), 1–6.
- [4] Lennert Appeltant, Guy Van der Sande, Jan Danckaert, and Ingo Fischer. 2014. Constructing optimized binary masks for reservoir computing with delay systems. *Scientific Reports* 4, 1 (2014), 1–5.
- [5] Janier Arias-García, Ricardo Pezzuol Jacobi, Carlos H Llanos, and Mauricio Ayala-Rincón. 2011. A suitable FPGA implementation of floating-point matrix inversion based on Gauss-Jordan elimination. In *Southern Conference on Programmable Logic*. IEEE, 263–268.
- [6] Filippo Maria Bianchi, Simone Scardapane, Sigurd Løkse, and Robert Jenssen. 2020. Reservoir computing approaches for representation and classification of multivariate time series. *IEEE Transactions on Neural Networks and Learning Systems* 32, 5 (2020), 2169–2179.
- [7] Jérémie Cabessa, Hugo Hernault, Heechang Kim, Yves Lamonato, and Yariv Z Levy. 2021. Efficient text classification with echo state networks. In *International Joint Conference on Neural Networks*. 1–8.
- [8] Keyan Cao, Yefan Liu, Gongjie Meng, and Qimeng Sun. 2020. An overview on edge computing research. *IEEE Access* 8 (2020), 85714–85728.
- [9] Huanhuan Chen, Fengzhen Tang, Peter Tino, and Xin Yao. 2013. Model-based kernel for efficient time series analysis. In *Proceedings of ACM International Conference on Knowledge Discovery and Data Mining*. 392–400.

- [10] Sosei Ikeda, Hiromitsu Awano, and Takashi Sato. 2022. Hardware-Friendly Delayed-Feedback Reservoir for Multivariate Time-Series Classification. *IEEE Transactions on Computer-Aided Design of Integrated Circuits and Systems* 41, 11 (2022), 3650–3660. <https://doi.org/10.1109/TCAD.2022.3197488>
- [11] Sosei Ikeda, Hiromitsu Awano, and Takashi Sato. 2023. Modular DFR: digital delayed feedback reservoir model for enhancing design flexibility. *ACM Transactions on Embedded Computing Systems* 22, 5s, Article 110 (sep 2023).
- [12] Hassan Ismail Fawaz, Germain Forestier, Jonathan Weber, Lhassane Idoumghar, and Pierre-Alain Muller. 2019. Deep learning for time series classification: a review. *Data Mining and Knowledge Discovery* 33, 4 (2019), 917–963.
- [13] Laurent Larger, Miguel C Soriano, Daniel Brunner, Lennert Appeltant, Jose M Gutiérrez, Luis Pesquera, Claudio R Mirasso, and Ingo Fischer. 2012. Photonic information processing beyond Turing: an optoelectronic implementation of reservoir computing. *Optics Express* 20, 3 (2012), 3241–3249.
- [14] Mantas Lukoševičius and Herbert Jaeger. 2009. Reservoir computing approaches to recurrent neural network training. *Computer Science Review* 3, 3 (2009), 127–149.
- [15] Michael C Mackey and Leon Glass. 1977. Oscillation and chaos in physiological control systems. *Science* 197, 4300 (1977), 287–289.
- [16] Mitsumasa Nakajima, Katsuma Inoue, Kenji Tanaka, Yasuo Kuniyoshi, Toshikazu Hashimoto, and Kohei Nakajima. 2022. Physical deep learning with biologically inspired training method: gradient-free approach for physical hardware. *Nature Communications* 13, 1 (2022), 7847.
- [17] Razvan Pascanu, Jack W Stokes, Hermineh Sanossian, Mady Marinescu, and Anil Thomas. 2015. Malware classification with recurrent networks. In *IEEE International Conference on Acoustics, Speech and Signal Processing*. 1916–1920.
- [18] Joan Serrà, Santiago Pascual, and Alexandros Karatzoglou. 2018. Towards a Universal Neural Network Encoder for Time Series. In *Current Challenges, New Trends and Applications*. 120–129.
- [19] Osaze Shears, Kangjun Bai, Lingjia Liu, and Yang Yi. 2021. A Hybrid FPGA-ASIC Delayed Feedback Reservoir System to Enable Spectrum Sensing/Sharing for Low Power IoT Devices. In *IEEE/ACM International Conference On Computer Aided Design*. 1–9.
- [20] Miguel C Soriano, Silvia Ortín, Lars Keuninckx, Lennert Appeltant, Jan Danckaert, Luis Pesquera, and Guy Van der Sande. 2014. Delay-based reservoir computing: noise effects in a combined analog and digital implementation. *IEEE Transactions on Neural Networks and Learning Systems* 26, 2 (2014), 388–393.
- [21] Gouhei Tanaka, Toshiyuki Yamane, Jean Benoit Héroux, Ryosho Nakane, Naoki Kanazawa, Seiji Takeda, Hidetoshi Numata, Daiju Nakano, and Akira Hirose. 2019. Recent advances in physical reservoir computing: A review. *Neural Networks* 115 (2019), 100–123.
- [22] Pattreeya Tanisaro and Gunther Heidemann. 2016. Time series classification using time warping invariant echo state networks. In *IEEE International Conference on Machine Learning and Applications*. 831–836.
- [23] Zhiguang Wang, Weizhong Yan, and Tim Oates. 2017. Time series classification from scratch with deep neural networks: A strong baseline. In *International Joint Conference on Neural Networks*. 1578–1585.
- [24] Bendong Zhao, Huanzhang Lu, Shangfeng Chen, Junliang Liu, and Dongya Wu. 2017. Convolutional neural networks for time series classification. *Journal of Systems Engineering and Electronics* 28, 1 (2017), 162–169.
- [25] Yi Zheng, Qi Liu, Enhong Chen, Yong Ge, and J Leon Zhao. 2014. Time series classification using multi-channels deep convolutional neural networks. In *International Conference on Web-Age Information Management*. 298–310.

Received 00 January 0000; revised 00 January 0000; accepted 00 January 0000